Article

Using Unmanned Aerial Vehicles (UAV) for High-Resolution Reconstruction of Topography: The Structure from Motion Approach on Coastal Environments

Francesco Mancini [1],*, Marco Dubbini [2], Mario Gattelli [3], Francesco Stecchi [4], Stefano Fabbri [4] and Giovanni Gabbianelli [4]

[1] DICATECh, Technical University of Bari, via Edoardo Orabona 4, I-70125 Bari, Italy
[2] DiSCi, University of Bologna, Piazza San Giovanni in Monte 2, I-40124 Bologna, Italy;
    E-Mail: marco.dubbini@unibo.it
[3] SAL Engineering, via Vittorio Veneto 2, I-41124 Modena, Italy;
    E-Mail: mgattelli@salengineering.it
[4] BiGeA, University of Bologna, via Sant'Alberto 163, I-48123 Ravenna, Italy;
    E-Mails: francesco.stecchi2@unibo.it (F.S.); stefano.fabbri21@unibo.it (S.F.);
    giovanni.gabbianelli@unibo.it (G.G.)

* Author to whom correspondence should be addressed; E-Mail: f.mancini@poliba.it;
    Tel.: +39-080-596-3399; Fax: +39-080-596-3414.

Abstract: The availability of high-resolution Digital Surface Models of coastal environments is of increasing interest for scientists involved in the study of the coastal system processes. Among the range of terrestrial and aerial methods available to produce such a dataset, this study tests the utility of the Structure from Motion (SfM) approach to low-altitude aerial imageries collected by Unmanned Aerial Vehicle (UAV). The SfM image-based approach was selected whilst searching for a rapid, inexpensive, and highly automated method, able to produce 3D information from unstructured aerial images. In particular, it was used to generate a dense point cloud and successively a high-resolution Digital Surface Models (DSM) of a beach dune system in Marina di Ravenna (Italy). The quality of the elevation dataset produced by the UAV-SfM was initially evaluated by comparison with point cloud generated by a Terrestrial Laser Scanning (TLS) surveys. Such a comparison served to highlight an average difference in the vertical values of 0.05 m (RMS = 0.19 m). However, although the points cloud comparison is the best approach to investigate the absolute or relative correspondence between UAV and TLS

methods, the assessment of geomorphic features is usually based on multi-temporal surfaces analysis, where an interpolation process is required. DSMs were therefore generated from UAV and TLS points clouds and vertical absolute accuracies assessed by comparison with a Global Navigation Satellite System (GNSS) survey. The vertical comparison of UAV and TLS DSMs with respect to GNSS measurements pointed out an average distance at cm-level (RMS = 0.011 m). The successive point by point direct comparison between UAV and TLS elevations show a very small average distance, 0.015 m, with RMS = 0.220 m. Larger values are encountered in areas where sudden changes in topography are present. The UAV-based approach was demonstrated to be a straightforward one and accuracy of the vertical dataset was comparable with results obtained by TLS technology.

Keywords: UAV; structure from motion; terrestrial laser scanning; digital surface model; beach dunes system

1. Introduction

The availability of Digital Surface Models (DSM) at high spatial resolution and vertical accuracy is of increasing importance for all sciences interested in the three-dimensional reconstruction of the environment. Among these, coastal geomorphology requires increasingly accurate topographic information of the so-called beach systems to perform reliable simulation of coastal erosion, flooding phenomena, and assessment of the coastal sediment budget. For such studies the availability of a topographic dataset is fundamental in particular for those systems characterized by a complex morphology. The presence of dunes has to be considered very carefully due to their role in coastal defense as protective natural features, providing sediment supply to beaches and protecting the inland from storm surges. Several studies have also demonstrated the relationship between dunes and ground saltwater intrusion [1,2], highlighting the importance of dunes for coastal agriculture systems. Nonetheless, the severe coastal erosion affecting numerous beaches and dune systems around the world is a large threat to their stability. Thus, for reliable modeling of the dune-beach system, including the behavior related to weather and marine conditions, detailed knowledge of the dunes' morphometry is necessary.

Despite the wide range of methods available for the production of high resolution point clouds, and successive high quality DSMs, some difficulties are generally experienced when topographic surveys are being carried out on the sandy littoral, based on significant investment in personnel and time, and the lack of benchmarks or other local permanent references. The latter are needed, in particular, to guarantee the georeferencing of point clouds within studies related to change analysis, where successive surveys have to be compared. These difficulties are a limiting factor for ground-based survey methods whenever a high spatial resolution and high quality DSM is required. Among the methods of suitable quality, devoted to the reconstruction of shore regions or dunes morphometry, those based on Global Navigation Satellite Systems (GNSS), total station and Terrestrial Laser Scanning (TLS) have to be mentioned [3–5]. GNSS positioning (based on Network or traditional Real

Time Kinematic) is fast and accurate, but limited in the number of measurable points. TLS can be very accurate, but requires long survey sessions due to dune anisotropy and significant investment in data processing time. Geomorphic studies based on airborne LIDAR (LIght Detection And Ranging) surveys are also relevant to this topic and can be found described in literature [6–9]. However, despite LIDAR's capacity to explore significantly extensive areas, its use is costly and results do not provide data with a comparable spatial and vertical accuracy with respect to TLS and GNSS. In order to overcome the limitations of the mentioned methods, the Unmanned Aerial Vehicle (UAV) based proximity survey for 3D reconstruction of coastal environments is being currently investigated. In particular, the use of the Structure from Motion (SfM) approach is an alternative to the classical digital photogrammetry approach based on the structured acquisition of images. SfM methods, initially developed within the computer vision process, refer to image-to-image registration methods for surface restitution with an ability to reach a higher level of automation and greater ease of use. A detailed explanation of the SfM process goes beyond the scope of this manuscript and the readers can refer to Snavely *et al.* [10], Snavely [11], and Ullman [12] for a detailed discussion on SfM. However, as SfM is more common in computer vision sciences, the description of some differences to the traditional digital photogrammetry used in geomatic disciplines will be briefly provided. As in many computer vision processes, the objective of the SfM strategy is to reconstruct 3D scene geometry and (sometimes not calibrated) camera motion from a set of images of a static scene by matching features on multiple images [13,14]. These methods are based on a new generation of image-matching algorithms applicable to unstructured image acquisition. On the contrary, a well-defined design of the images acquisition phase is a prerequisite of classical photogrammetry [15–18]. Due to such reasons, the SfM approach resulted in great interest in the processing of images acquired by multi-rotors UAVs, where irregularities often experienced in the path followed by the vehicle, varying altitude, and camera attitude could constitute a benefit. This is due to the ability of the latest image-matching algorithms to recognize a very large number of conjugate features over a set of multiple images acquired by an aerial vehicle flying at a very low altitude. Such algorithms are based on a multi view approach. The redundancy of acquisitions guarantees the success of the processing even for images acquired by variable attitude of the imaging system, causing changes in view point, image scale, or resolution [19].

On a positive note, the automated image-matching phase allows the SfM to solve the collinearity equations in an arbitrarily scaled coordinate system, without any initial requirements regarding the knowledge of Ground Control Points (GCPs). After the collinearity equations are solved, software implementing the SfM workflow generates, as intermediate products, a point cloud of X, Y, and Z positions, which is not registered to any cartographic or local reference system. Further, the dense stereo-reconstruction techniques do not require initial information about location and attitude of the imaging system. Such could be the case of a UAV survey carried out under emergency conditions, without a well-defined flight plan or in the absence of known GCPs within the investigated area. Rango *et al.* [20] found that the traditional photogrammetry workflow is sometimes difficult for unconstrained imagery acquired from a powered UAV system. For all the above reasons, the point cloud generation by SfM methodology was selected as appropriate for the case study. Based on the complexity of the available algorithms, two alternative solutions to frame the SfM point cloud to the reference system of the GCPs are possible; the classical rigid 7-parameters Helmert transformation and the bundle adjustment procedure. The Helmert transformation relies on a linear procedure and any

non-linear distortions, introduced by errors in the automated matching process, will affect the 3D products and cannot be removed. Whenever a rigid transformation is performed, a crucial assumption is therefore accepted in the SfM; the automated image matching process produces none or little non-linear deformation [19]. Due to this assumption a rigorous geometric validation on 3D products from SfM approaches is required on the whole extent of the imaged object.

In the field of 3D reconstruction from proximity images and SfM methods, results obtained by Verhoeven [21] and Verhoeven *et al.* [22] using low-altitude helikites in archaeology could be cited. Mathews and Jensen [23] and d'Oleire-Oltmanns *et al.* [24] addressed issues related to vineyard and soil erosion, whilst Wallace *et al* [25] and Hunt *et al.* [26] used UAV data for studies of forestry and agriculture. Fonstad and Marcus [27], Houser *et al.* [7], and Turner *et al.* [28] report applications to topography whereas Harwin and Lucieer [29] assess the quality of results on coastal environments. A complete comparative study on performances, achieved by traditional photogrammetry and image-based approaches, is provided by Rosnell and Honkavaara [30].

These authors prove the reliability of DSMs obtained from UAV-SfM for the study of several natural environments. In literature, very few experiences about reconstruction of topographic features by UAV-SfM deal with sandy littorals and coastal dunes. The paper by Harwin and Lucieer [29] investigated the accuracy of point clouds generated from UAV imagery of coastal environment, by comparison with a discrete set of validation points gathered by a total station. Recently, Bryson *et al.* [31] used kite aerial photography and SfM to study intertidal rocky landscapes with quantification of relative accuracy of final products. Nevertheless, the assessment of absolute accuracy of point clouds and DSMs derived from UAV imagery on sandy coastal environments needs additional validation procedures. Tidal flats, beaches and dune systems exhibit different tonal contrast in images acquired by a proximity aerial survey with the possibility of such responses being related to the dominant grain size or to the presence of coastal dune vegetation. All these features contribute to the variable reliability of the products obtained by the processing of high-resolution images from UAV platform, and a quantitative study of accuracy of these products could be of interest for the scientific community. This paper presents a comparative study of this methods' accuracy and that of a terrestrial laser scanning solution. The validation of reconstructed surfaces is a fundamental issue as erroneous 3D product can profoundly influence experts' decision based on interpretation of surface features. Such validation is also important for single or multitemporal elevation dataset that serve as input data for numerical models, such DSMs used in sediment budgeting models [7,32].
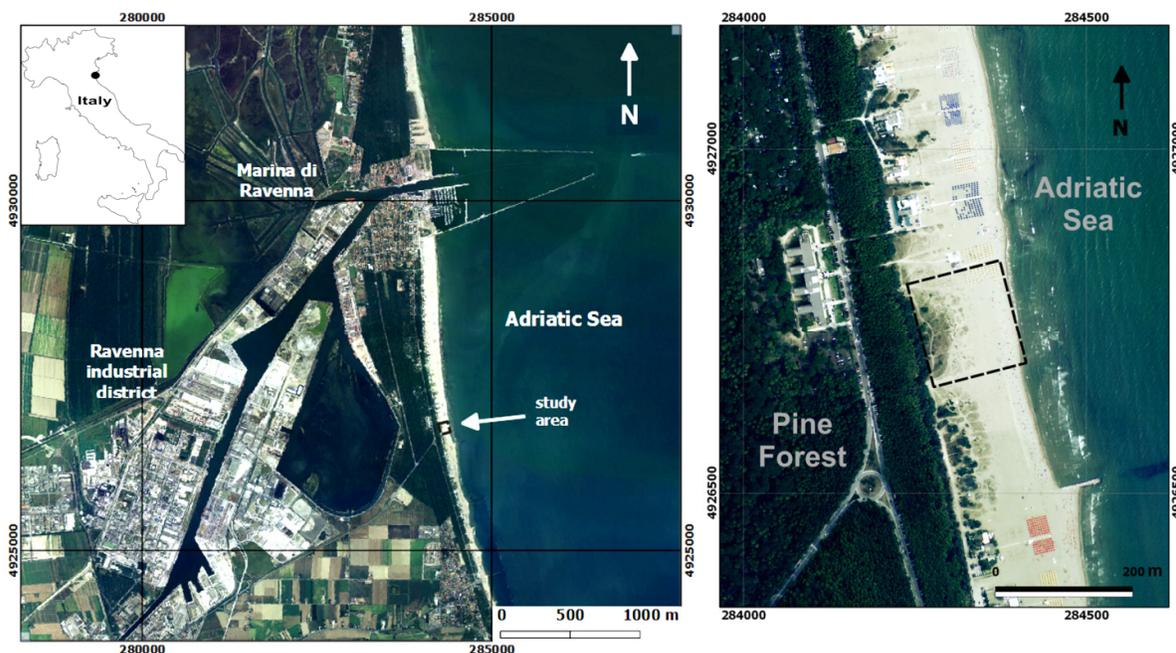
This study aims at the creation and validation of point cloud and DSM of a complex beach dune system.

2. Study Area

The investigation concerns a fore-dune located in Ravenna (Italy), on the North Adriatic coast, an area characterized by reclaimed low lands and wetlands typical for delta areas within the alluvial Po Plain. The Ravenna coastal stretch, extending for less than 40 km in the N-S direction, is characterized by the presence of naturalistic sites and equipped sandy beaches, sometimes bordered by pine-forests, and proximate urban areas. Almost all this area is affected by an erosive trend as a consequence of several factors, such as strong reduction of rivers' sediment supply, destruction of dunes systems by tourism-related pressures, establishment of harbors and piers affecting the normal alongshore sediment

drift, significant land subsidence [33], ineffective defense structures, and sea level rise [34]. Coastal vulnerability assessment of this area is currently of great interest because of the importance of the coast for tourism-generated economy, a significant resource for the local community during the summer season. The natural dune system has been acknowledged as a fundamental protective feature and the local Municipality has promoted the creation of a detailed 3D dunes inventory. Among methods able to perform such a survey, the processing of images acquired by multi-rotor UAVs was tested for a confined 200 m wide dune patch found along the coastal resort area of Marina di Ravenna (see Figure 1). It was selected as a test site due to its very complex topographic features, presence of weathering features, and relevance of its protective role towards the inland.

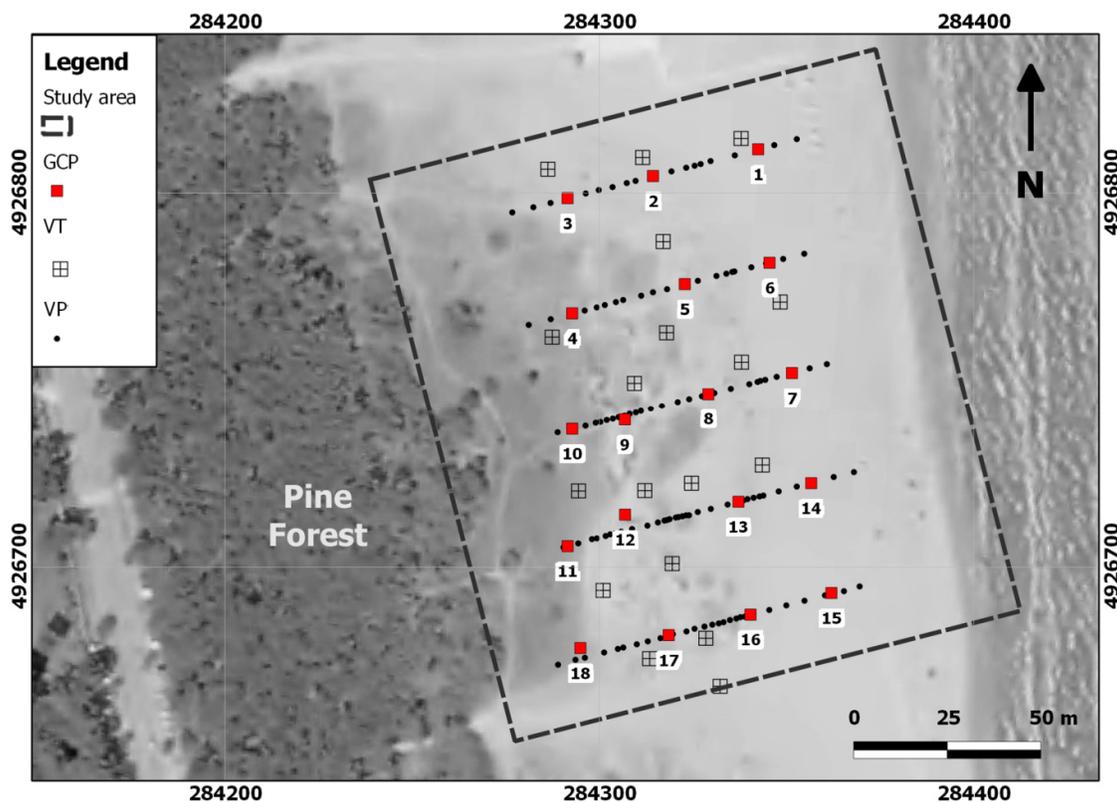**Figure 1.** Location map of the study area. The dashed rectangle encloses the surveyed zone.

3. Methodology: GNSS, UAV, and TLS Surveys

3.1. Ground Truths: the Global Navigation Satellite System (GNSS) Survey

A Networked Real Time Kinematic (NRTK) survey using the Virtual Reference Station (VRS) solution was carried out on 27 May 2013, together with data acquisition by Terrestrial Laser Scanning (TLS) and UAV flight. The NRTK survey had a threefold point collection purpose. Eighteen 3D Ground Control Points (GCP) consisting of cubes (30 × 40 × 30 cm) with a 20 cm wide chessboard printed on the upper side, 126 Validation Points (VP) at surface ground level along five transects evenly distributed across the dune extent, and 19 Vertical Targets (VT) designed to georeference and merge the TLS acquisitions. The GNSS-NRTK survey, performed by a dual frequency GRS1 (Topcon) for the mentioned dataset (GCPs, VPs, and VTs), resulted in RMS values of less than 0.018 m and 0.029 m for horizontal and vertical accuracies respectively, for 99% of the sampled points. Horizontal coordinates were referenced to UTM Zone 33N (ETRF00), while the vertical values were also referred to the mean sea level using the geoid model ITALGEO2005 provided by the Italian Geographic

Military Institute (IGMI). Locations the distribution of GCPs, VPs, and VTs positions used in this study, as well as simple sketches of GCPs and VTs can be seen in Figure 2.

> **Figure 2.** Set of GNSS locations used in this paper as reference for the employed methodologies. Ground Control Points (GCP): used as reference in the bundle adjustment of cloud point from UAV-SfM procedure (numbered for successive uses); Validation Points (VP): ground points used as reference for validation of the UAV and TLS-derived elevation dataset; Vertical Targets (VT): useful for georeferencing of TLS points. The dune system is included within the black dashed line.

3.2. The Unmanned Aerial Vehicle (UAV): Technical Specification and Survey

The UAV system used was a VTOL (Vertical Take Off and Landing) hexacopter designed and manufactured by SAL (Sea Air Land) Engineering and equipped with a calibrated Canon EOS model 550D digital camera. Table 1 lists some technical specifications of the UAV system whereas Figure 3 depicts the entire equipment.

The survey lines were planned using an aerial orthophoto at an average flight altitude of 40 m and acquisition was automatic set on one shot per second. The redundant set of images acquired at the selected timing facilitates the SfM approach. Images acquired during the take-off and landing operations were filtered out during the successive processing. The take-off and landing operations were manually driven by a remote pilot. During the survey the automatic flight through waypoints was enabled. Wind was blowing at an average speed of 10 knots with gusts of up to 18 knots. This resulted in horizontal deviations of up to 10 m and vertical deviations of up to 5 m. The flight time was of 7

minutes at an average speed of 4 m/s and the final aerial dataset resulted in more than 800 images of which 550 were selected following successive data processing. The acquisition timing gave up to 10 overlapping images for any single ground feature and any attempt to illustrate the coverage of the aerial images for such a limited area would result in a rather confused figure.

Table 1. Some key specifications of the Unmanned Aerial Vehicle (UAV) system.

Manufacturer	S.A.L. Engineering, Modena, Italy
Type	Micro-drone Hexacopter
Engine Power	6 Electric Brushless
Dimension and weight	100 cm, 3.3 kg (total weight for all equipment is approximately 5 kg)
Flight mode	Dual, automatic based on waypoints or base on wireless control
Endurance	Standard 20 min (+5 min safety)
Flexible camera configurations	Digital gimbal, Canon EOS 550D (focal length 27 mm), res. 5184 × 3456 Bi-axial roll and pitch control
Ground Control Station	8-channels, UHF modem, telemetry for real time flight control, and path tracking on video within 5 km

Figure 3. The UAV hexacopter (reference length in figure: 1 m).

3.3. The Terrestrial Laser Scanner Survey

Contemporary to the GNSS survey, a reference DSM of the dune system was created through a data collection by a phase based TLS survey with a CAM2 Focus3D system. This data acquisition phase was a part of a research project endorsed by the local municipality to fulfill the littoral protection plan through an initial inventory of the exiting dune systems and successive actions oriented towards the preservation. A total of 18 scans characterized by a point resolution of 7.7 mm at 10 m (3 average measures per point) were acquired and registered by a set of 19 georeferenced VTs consisting of B/W 50 cm square chessboards installed on a 1.5 m pole. Target centers were measured via GNSS-NRTK

technology, considering the proper antenna offsets. The intense sunlight led to reduced TLS efficiency and increased the scattering phenomena, leading to reduced measuring distance and lower accuracy.

3.4. Software

The processing of original image collection was performed by the software package called PhotoScan, available at a moderate cost for research institutions from the Russian manufacturer AgiSoft LLC [35]. The simple and straightforward interface in addition to state-of-the-art routines from the computer vision environment, make this package a candidate for fast and effective processing of remotely sensed data. The SfM algorithm implemented by PhotoScan was used in this work to generate the dense DSM of the study area to be successively validated with the GNSS GCPs and compared with the DSM produced by the more familiar TLS survey technique. The reconstruction of ground surface and objects by PhotoScan is a three-step process [36]. For a good reconstruction, at least two photographs representing a single point must be available [35,37].

In the first step the alignment of the acquired images was performed. The SfM algorithm comes into play by the detection of image feature points (edges or others geometrical features) and reconstruction of their movement along the sequence of images. The SfM algorithm provides the basic geometry/structure of the scene, through the position of the numerous matched features, in addition to camera positions [37] and internal calibration parameters. In the second step a pixel-based dense stereo reconstruction was performed starting from the aligned dataset [36]. After this step, fine topographic details available on the original images could be meshed. Amongst available stereo matching procedures implemented in PhotoScan, the Height Field is recommended for aerial surveys [38]. In the third step a texturing was applied to the mesh. Despite the good level of automation of the whole procedure, the computation could be time consuming or limited by the amount of RAM available. The point cloud was then shaped and referenced to a local coordinate system. Successively, the point cloud was framed in the UTM coordinates system. For this step, the bundle adjustment procedure was chosen over the similarity seven-parameter transformation, since it was known to produce more accurate results, despite possibly higher time consumption, this depending on the number of image acquisitions.

4. Results

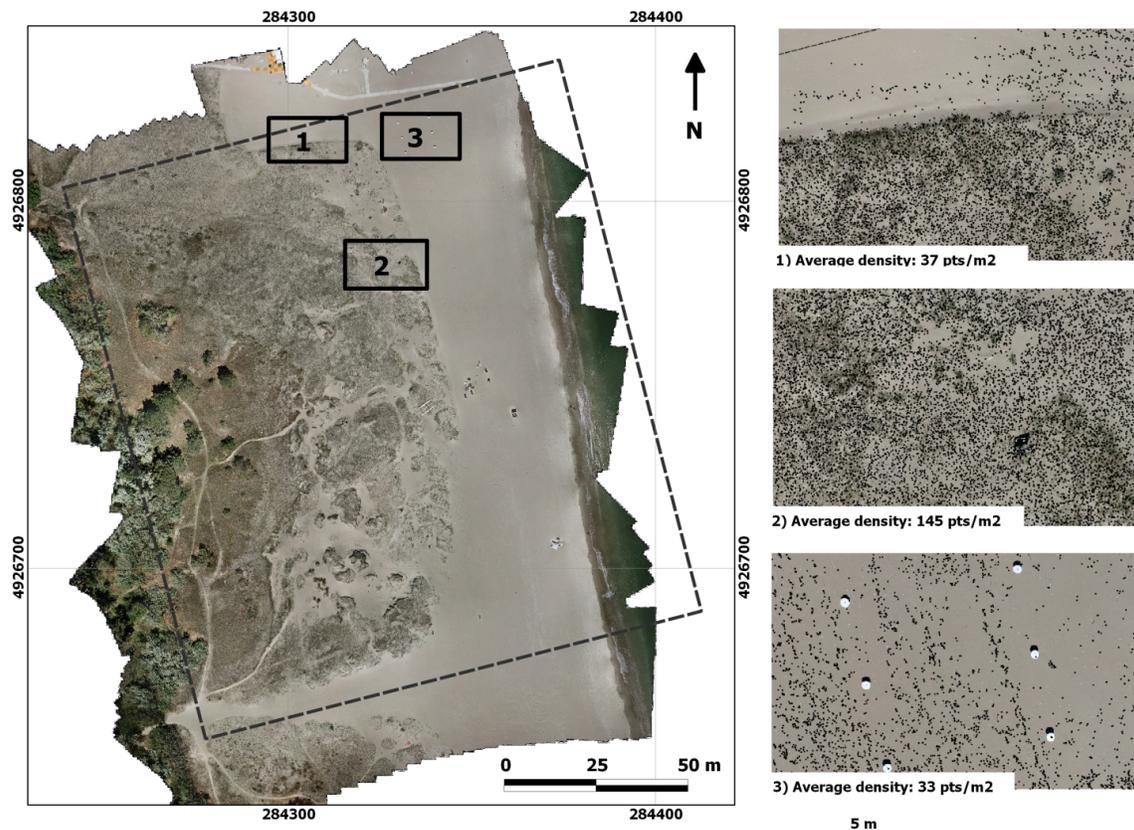*4.1. Point Cloud and DSM from UAV Images*

The initial processing of 550 images (ground resolution of 0.006 m/pixel at 40 m flying height) acquired by the UAV system, through the features-matching procedure implemented in the SfM algorithm, produced a point cloud consisting of 831,153 features in the arbitrarily scaled coordinate system over an area of 27,500 m^2.

By knowledge of the GCPs coordinates, after processing by the SfM approach, bundle adjustment was performed to register the model in the UTM reference system Camera locations and attitude were considered as unknowns. The bundle adjustment was based on a sub-set of 10 GCPs uniformly distributed over the study area and with respect to corresponding GCPs, the whole transformation resulted in RMS values of 0.008 m in the East direction, 0.007 m in the North direction, 0.077 in the vertical direction, and 0.078 m within the 3D component (see Table 2).

Table 2. Residuals of the bundle adjustment transformation on used Ground Control Points (GCPs) and total errors (m).

GCP	UTM Coord (m)			Individual Residuals after the Transformation (m)			
	East	North	Elev.	East	North	Elev.	3D
1	284342.420	4926811.730	1.900	0.005	0.000	−0.023	0.024
3	284291.510	4926798.710	2.720	0.022	0.016	0.160	0.162
4	284292.740	4926768.000	3.760	0.001	0.002	−0.004	0.005
5	284322.820	4926775.800	2.770	−0.005	0.009	−0.081	0.082
7	284351.450	4926752.100	2.020	0.001	0.007	−0.010	0.012
10	284292.760	4926737.020	2.890	−0.007	0.000	−0.153	0.153
13	284337.150	4926717.480	3.130	−0.004	0.000	−0.020	0.020
14	284356.590	4926722.440	1.970	0.001	−0.001	0.005	0.005
15	284361.990	4926693.110	2.020	0.000	0.002	0.058	0.058
18	284294.940	4926678.390	3.500	−0.004	−0.006	−0.008	0.011
			RMS	0.008	0.007	0.077	0.078

Figure 4. Point density on three different surface types in image windows of 10 m × 7 m. The orthophoto (**left**) produced by the UAV survey is used as reference image. Average point density is reported.
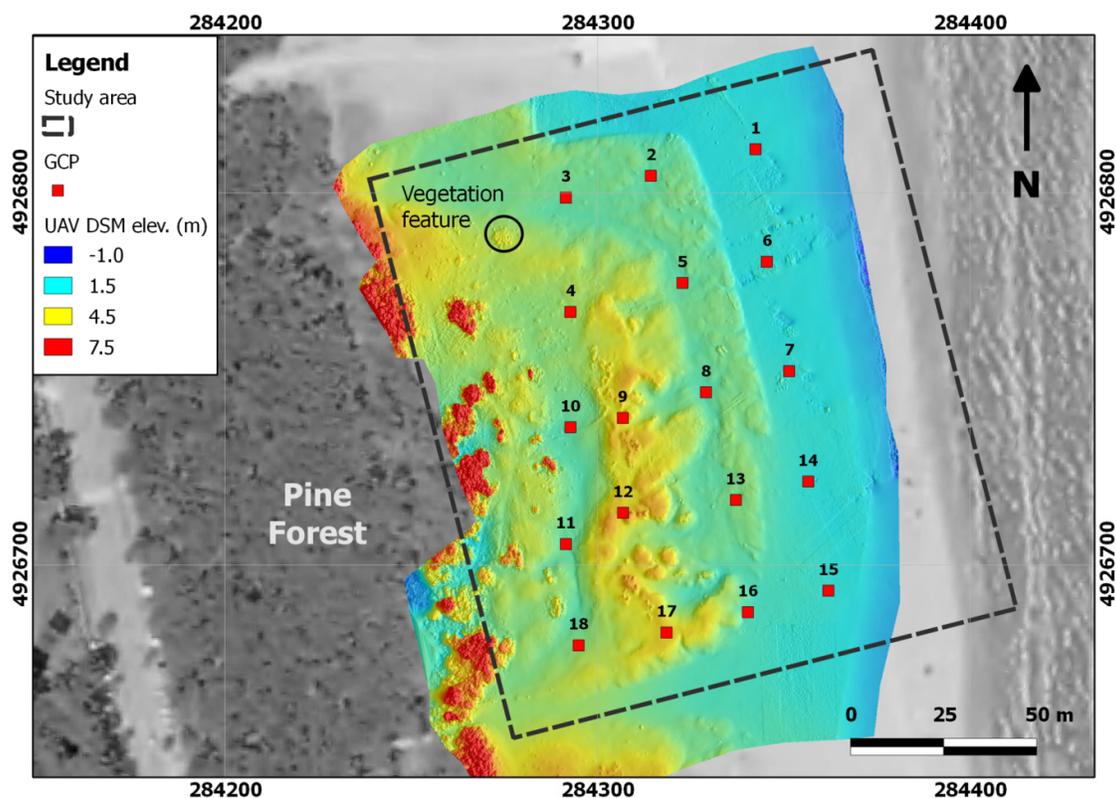

The planimetric error of the adjustment resulted to be almost negligible (less than 1 cm) whereas the vertical accuracy in a couple of points (3 and 10) exhibited less favorable outcomes (around 15 cm

differences). The vertical RMS of the bundle adjustment amounts to 7.7 cm, also strongly influenced by residuals detected at points 3 and 10. For a better understanding of the relation between point density and three different surface types within the study area, the pattern of points produced from the features-matching algorithm are represented in Figure 4. Zone 1 shows two very distinct features. The upper part includes flat area with sands, the lower section represents the body of the dune where sands are coarser, slope increases, and very low and sparse dune vegetation can be detected. Zone 2 almost entirely represents the body of dune and zone 3 shows a completely flat area with sands and supports for umbrellas used during the tourist season.

The point density calculated for zone 3 is lower than the value pertaining to zone 2. This is due to difficulties of the features matching algorithm to relate features for homogenous textures.

Successively, for further investigations on the absolute accuracy of 3D surface from the point cloud, a linear interpolator was used to produce a DSM. The pixel spacing was selected on the basis of the average distance between points of the cloud within denser areas (see for example the average density of zone 2). This resulted in an 8 cm resolution DSM leading to a densification of points for areas where the density of points was minor. The resulting DSM is represented in Figure 5.

Figure 5. Hillshaded DSM from UAV survey with elevations above sea level (m) and locations of available GCPs.

The meshed DSM shows a fine representation of the elevation dataset over the study area. Patches with elevations of over 7.5 m are known to represent vegetated areas. Consequently, such features were not included in the successive validation process or in the comparison with the DSM derived using TLS methodology. Meanwhile, features representing sparse and low (15 to 20 cm) vegetation

patches (as the area encircled in Figure 5) were not removed from the DSM, with possible effects on successive comparisons evaluated.

4.2. Point Clouds and DSM from Terrestrial Laser Scanning (TLS) Survey

A total of 18 scans produced a point cloud composed of 115 million points. All the scans were registered in an absolute reference frame using the mentioned georeferenced VTs. After the adjustment procedure, residuals detected for common VTs were of a maximum value of 3 cm, in agreement with the global accuracy related to the GNSS survey of reference points.
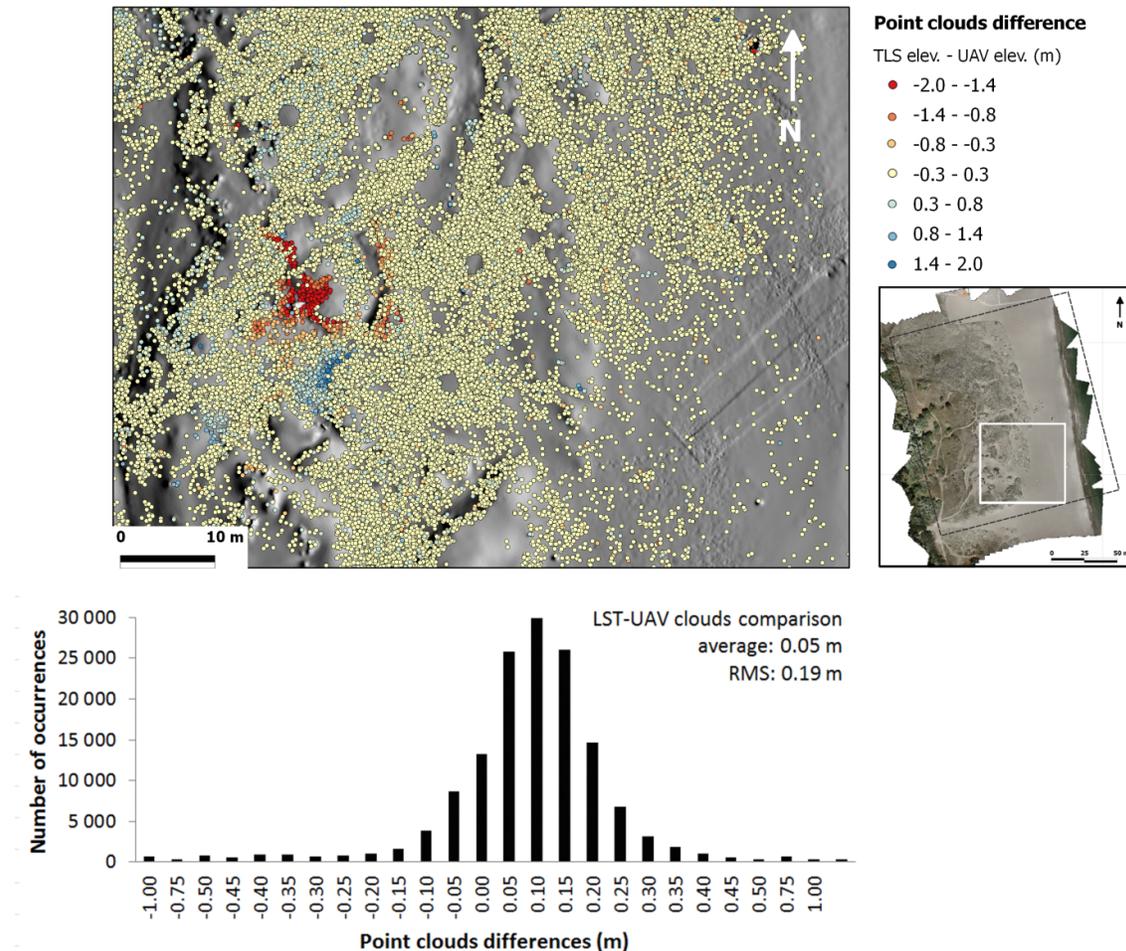
After this basic data processing a meshed surface was created avoiding any smoothing procedure. A grid of 4 cm resolution was exported to be validated by GNSS positions and successively compared with the DSM generated by the UAV survey and SfM approach. This spacing was derived from the average density of points within areas characterized by a scarce response to the incoming laser beam. As in the SfM procedure, responses from low and sparse vegetation on some portions of the dune surface were not filtered out from the dataset. Due to a very similar appearance with respect to the DSM of Figure 5 at the scale of representation, this dataset is not being represented by any additional image.

4.3. UAV, TLS, and GNSS Comparisons

In order to evaluate overall quality and absolute positional accuracy of results from UAV-SfM in the reconstruction of the dune 3D surface by a proximity survey, a first comparison was performed with respect to the TLS-based point cloud. An absolute georeferencing procedure is a definite requirement whenever the evolution of coastal morphologies is to be investigated [39]. The georeferencing of these point clouds was based on NRTK GNSS survey used to locate Vertical Target (VT) and horizontal GCPs as reference for the TLS and UAV surveys respectively. Certainly, the comparison between point clouds is affected by the vertical accuracy achieved in the GNSS reference survey. TLS and the UAV-SfM point clouds differencing was performed by using a tool included in ArcGIS, *Spatial Join*, with *Closest* option (search radius set to 10 cm to compare closest points). Elevations of points of the UAV-SfM and TLS clouds are compared if their horizontal distance is less than 10 cm. Isolated points over both point clouds are not considered in this comparison. To avoid graphical confusion due to the numerosity and vicinity of compared points, results are plotted in Figure 6 for a subset of data corresponding to a sector where major values are present. The comparison procedure selected about 120,000 common points.

Figure 6 shows major positive and negative (up to 2 m) values within a very limited portion of the study area. Evidently, the point clouds are affected by errors due over this portion of the study area. Within this area, the comparison between dataset and reference elevations provided by the VPs shows that discrepancies are mainly related to wrong elevations in the TLS dataset. It corresponds to a sector where sudden changes in topography are present but problems in the TLS survey have unknown reasons. The average positive distance (0.05 m) could be related to a major sensitivity of the laser data capture method toward the presence of sparse vegetation. The RMS value (0.19 m) reflects a limited scattering of results due to limits of used approaches for such typology of surface.
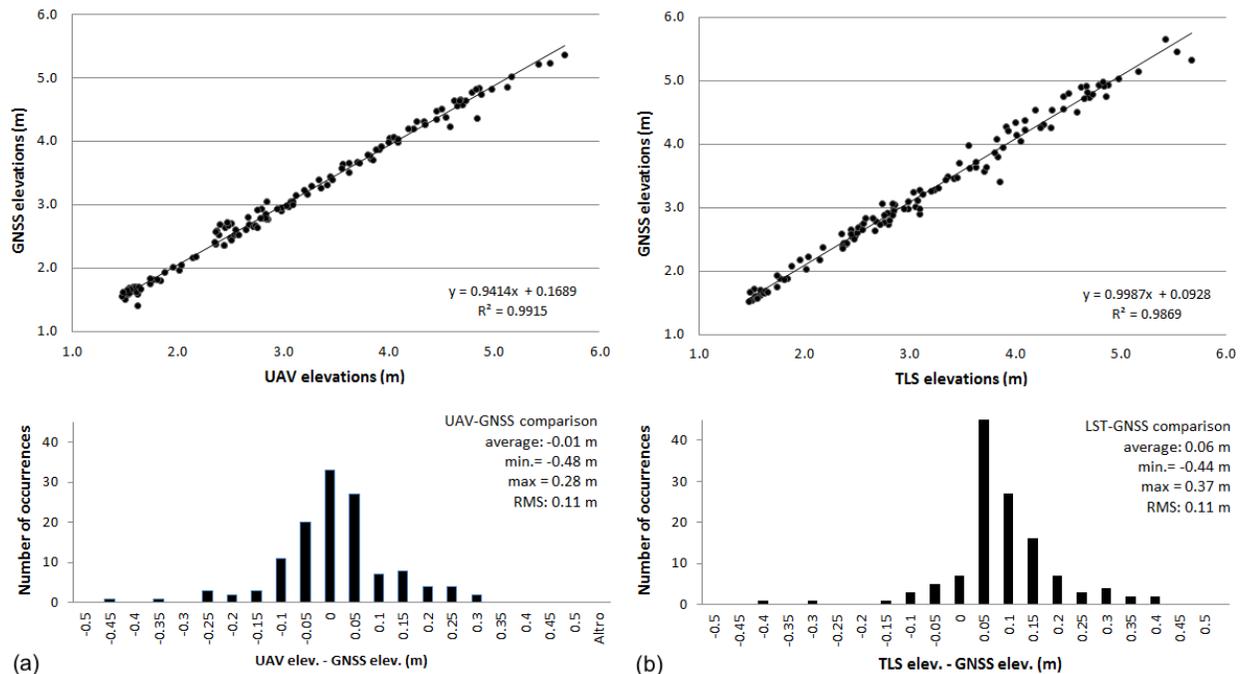
Figure 6. Points clouds comparison obtained by subtracting the UAV elevations from closest TLS elevations. Differences are represented by a color-coded solution over the shaded UAV DSM and frequency histogram of differences reported (statistic parameters referred to the whole dataset).

Further, even if the point clouds comparison is the best approach to investigate the correspondence of the UAV-SfM and TLS methods, the assessment of geomorphic features is usually based on surfaces analysis where an interpolation process is required. For this reason, a successive step was carried out, after interpolation, to compare the UAV-SfM and TLS DSMs with ground locations gathered along five transects equally spaced across the study area.

Thus, a quantitative assessment of absolute vertical differences between the DSMs, by UAV-SfM and TLS, was obtained by the comparison of surfaces and 126 GNSS VPs distributed along transects represented in Figure 2. More precisely, the vertical values corresponding to the location of VPs, for the UAV and TLS surface models, were sampled by the *point sampling tool* plugin available in Quantum GIS (1.8.0) the open source GIS software used in this work. Certainly this comparison could be influenced by artifacts related to the linear interpolator used for DSM production. In particular, this effect was visible within areas where point clouds show a smaller amount of data. Results are shown in Figure 7a,b.

Figure 7. Comparison between elevations of VPs surveyed by GNSS and corresponding points sampled from the DSMs. (**a**) Plot of the fit with linear regression parameters between VPs and UAV elevations (m) and related frequency histogram of differences. (**b**) Plot of the fit with linear regression parameters between VPs and TLS elevations (m) with related frequency histogram of differences.
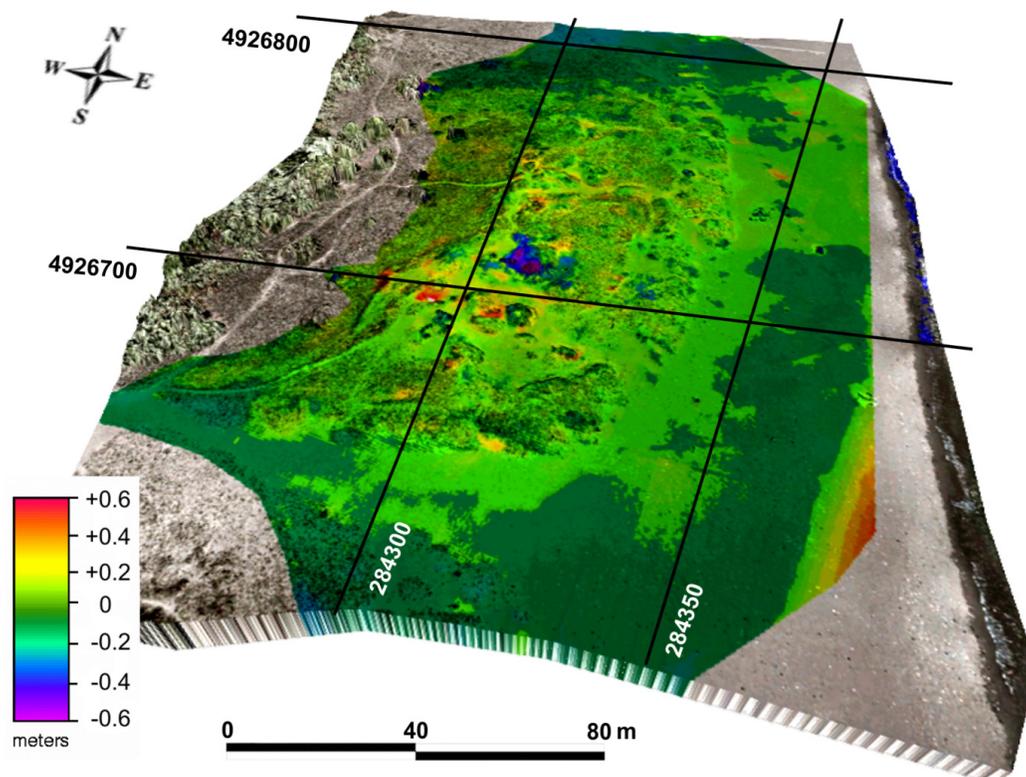

The average distance between UAV and GNSS elevations (−0.01 m) is concordant with the absolute accuracy provide by the GNSS positions used as reference points (less than 0.029 m on 99% of the sample). The RMS value (0.11 m) is affected by the presence of significant differences noticed on few VPs indicated by the tails of the frequency histograms. Additionally, these discrepancies could derive from the interpolation process of portions with low vegetation or ripples of a few centimeters in height. Moreover, differences in the RMS values could be due to the different way in which the ground elevations were computed: UAV elevations were based on image processing, whereas the GNSS values were collected by a hand rod resting on the ground. Further, considering the vertical RMS values related to the GNSS measurement, the validation procedure confirms the high performance of the SfM methods applied to images acquired by the UAV system. The regression line on Figure 7a shows a very good agreement of measurements and a near 1:1 fit between corresponding points. The deviation from the theoretical rate (unitary) is most likely due to a small scaling factor difference between the compared DSMs. In Figure 7b the same comparison was performed to validate the TLS DSM. Here, the average distance (0.06 m) is further from the global accuracy of the georeferencing procedure and the fit of the TLS-DSM and the GNSS reference positions are not as good as in Figure 7(a). The source of errors can be observed in the scatter plot in Figure 7b. It shows a better agreement at low elevations and more scattered points found at higher values. This is likely due to the logistic difficulties encountered during the TLS survey with respect to sudden changes on topography. Areas affected by this limitation are those shown on Figure 6. The second source of error for TLS data

could be related to the unmodeled presence of sparse and low vegetation. A systematic positive difference between TLS and UAV-SfM elevations could derive from the oblique data capture geometry of the laser sensing more sensitive toward the sporadic presence of vegetation or surface roughness. Nevertheless, the RMS error (0.11 m) is as in Figure 7(a). The frequency histograms show a quasi-Gaussian curve in the UAV-GNSS case and a moderately positive tail in the TLS-GNSS comparison. Meanwhile, the fit is very close to unity for both comparisons. In light of the above considerations, both surfaces have a very good level of vertical accuracy. In particular, the UAV-DSM exhibits an almost ideal behavior in comparison to the 126 VPs available after the GNSS survey. A similar test was carried out for a UAV-DSM produced by a similarity transformation without any bundle adjustment procedure (results not reported): the resulting average distance between GNSS and UAV elevations being of 6 cm with no difference in the RMS value.

The discrepancies between the UAV and TLS elevation surfaces were assessed by a point-by-point comparison. Both surfaces have very similar point densities but artifacts due to the interpolation processes could have had an effect on this comparison. The TLS survey covers a slightly reduced extent and the comparison area was reduced accordingly. The map of spatial error distribution between the UAV and TLS dataset is provided in the perspective view of Figure 8.

Figure 8. Spatial error distribution between DSMs obtained by subtracting the UAV elevations from TLS elevations. Differences are represented by a color-coded solution over the high-resolution orthophoto produced after the UAV survey.

As can be seen from Figure 8, the elevation differences are almost neutral all over the investigated area (green tones) but, as seen in the point clouds comparison, where sudden changes on topographic

features are encountered the vertical differences exhibit higher values. See, for example, the red and blue-violet areas in figure, where extreme values of the color-coded bar are encountered. Such differences were also detected by the clouds comparison from UAV-SfM and TLS (see Figure 6). The smoothing effect on point clouds introduced by the interpolator is also visible for this area by the decreasing of absolute differences. More generally, the comparison shows a very small average distance between surfaces (0.015 m) and an RMS of 0.220 m. The average distance between surfaces is less than the average distance between point clouds. Again, the smoothing effect due to use of an interpolator could cause this effect by reducing the vertical scattering of points whenever an average surface is being generated. The RMS seems not much compatible with inaccuracies of original surfaces validated with GNSS data and increases in comparison to the RMS of point clouds validation. However, it is based on comparison of interpolated values, less reliable within areas characterized by lack of points, where outcomes of the interpolation can diverge from reality.

5. Discussion

The assessment of SfM performances from UAV imageries could be difficult for DSM representing a complex beach dune system. Areas characterized by "smooth" surfaces (snowy, sandy, or rocky areas) may be failure-prone because of possible difficulties by the matching algorithms to extract corresponding features over uniform surfaces [19,27]. It is the case for geomorphic studies applying proximity sensing for coastal geomorphology studies. Furthermore, Rango *et al.* [20] found that software designed to process aerial images by traditional digital photogrammetry is not well suited for unstructured image acquisition geometries. These motivations drew our attention to the use of SfM to derive and validate high-resolution topographic datasets. First of all, the SfM technique is an appealing one because of its easy-to-use, elevated degree of automation and less stringent requirements on image acquisition geometry and camera calibration. Further, in this study, it facilitated the production of a high definition DSM on sandy surfaces, where alternative surveys could have been precluded by the absence of local and stable ground references.

The validation procedure illustrated in this paper suggests that both methodologies, UAV-SfM and TLS, employed to generate point clouds and high resolution DSMs of the beach dune system, exhibit a very good degree of agreement with GNSS ground truths. These comparisons show average discrepancies at centimeters levels with related RMS of 22 cm as worst case. Point clouds and DSMs cross comparison shows a good agreement across the study area even though some discrepancies within areas with sudden changes of topography were detected. By using the GNSS measurements as reference, these discrepancies seem to be dependent from the TLS DSM, likely due to logistic difficulties in the data capture phase. The point cloud generated by UAV-SfM methodology exhibited different point density depending on the images textural properties. The average value for denser areas was used as reference spacing in the DSM exporting procedure. Results obtained from the validation procedure of DSMs from both methodologies could be a starting point whenever an accuracy assessment of 3D products is required. In the fulfillment of high resolutions DSMs costs are incomparable; the TLS survey is two or three orders of magnitude more expensive than a UAV one. Meanwhile a traditional topographic survey (by a total station) would be of similar cost to the UAV system, but the resulting DSM would be much coarser for a similar field-effort.

In this work, the redundant number of images acquired by the UAV proximity flight guaranteed a good success in the automated point matching and application of the SfM approach. This is because of the very high spatial resolution of images that facilitate the recognition of textures at the ground even for smooth and reflective surfaces. It is the case of bare sand. Especially, for such surface typology, a minimum number of 10 overlapping images should be acquired to allow a reliable automated matching procedure [19].

The average flight altitude (40 m from the ground) allowed good image definition and improved the overall quality of the orthophoto for further uses (including the analysis of dune vegetation by inspection of photographic products and recognition of geomorphic features). We found the use of the hexacopter UAV very effective for such a small study area free from obstructions where remote piloting can be realized under safe conditions. Some drawbacks on the use of UAV for sandy environments have to be highlighted. The take-off and landing operations are crucial because of the sand set in motion by rotors, unless a hard platform is used, and functionality of rotors and camera lens could be compromised by finer grains raised during such phases.

A bundle adjustment procedure based on a redundant number of GCPs was used. A total of 18 were located by GNSS measurements of which 10 were finally used. Following further testing, the number of GCPs used could be further decreased without significant loss of accuracy, reducing the effort for acquiring ground-based references for the georeferencing of SfM products. For UAVs with differential GNSS positioning [28] (not the case in this study) as camera locations are known and transformation from the relative to the absolute system is possible, aerial positions could be used instead of ground GCPs.

6. Conclusions

Results presented in this paper are promising and the workflow is characterized by an elevated degree of automation. The SfM technique applied to images acquired by a low-altitude UAV system produced a point cloud and derived DSM representing a beach dune system with high topographic quality and vertical accuracy, comparable with GNSS survey data. The absolute average distance between UAV-SfM surface model and GNSS data is within the uncertainty of reference positions and RMS at 10 cm level. Possible source of errors were introduced in this paper. In addition, the comparison with point cloud, and derived DSM, provided by TLS method shows absolute distances not larger than 5 cm and maximum RMS value of 22 cm. Nevertheless, in this comparative analysis we found some difficulties over a small area with sudden change of topographic slopes. By taking the GNSS data as reference for this area, the mentioned issues seem to be related to the TLS survey. Examples of quantitative applications of the SfM methodology to UAV images in literature are limited and a quality assessment is still a requirement for different geomorphic environments [24,27,31]. This may be accomplished through comparative studies between SfM-derived topographic datasets and datasets from other high-resolution methods, or from the less expensive GNSS survey of natural points or artificial targets evenly distributed on the area of interest. In spite of some unfavorable conditions of the case study (see discussion about uniform surfaces), SfM seems to be a powerful tool to process images acquired by the UAV system. The high degree of automation of the workflow and an absolute vertical accuracy at 20 cm level achieved by the DSMs suggest possible uses in the fields of natural

hazards, disaster response and high-resolution terrain analysis. However, whenever a DSM is derived from sparse clouds and used within a model, effects introduced by the interpolation process have to be addressed very carefully and a reliable uncertainty value assigned to the elevation dataset. Beyond that, all circumstances requiring fast access to quantitative and qualitative data could benefit from the use of such a technology.

Conflicts of Interest

The authors declare no conflict of interest.

References

1. Giambastiani, B.M.S.; Antonellini, M.; Gualbert, H.P.; Essink, O.; Stuurman, R.J. Saltwater intrusion in the unconfined coastal aquifer of Ravenna (Italy): A numerical model. *J. Hydrol.* **2007**, *340*, 91–104.
2. Chen, J.S.; Li, L.; Wang, J.Y.; Barry, D.A.; Sheng, X.F.; Gu, W.Z.; Zhao, X.; Chen, L. Water resources: Groundwater maintains dune landscape. *Nature* **2004**, *432*, 459–460.
3. Brodu, N.; Lague, D. 3D Terrestrial lidar data classification of complex natural scenes using a multi-scale dimensionality criterion: Applications in geomorphology. *ISPRS J. Photogramm. Remote Sens.* **2012**, *68*, 121–134.
4. Nield, J.M.; Wiggs, G.F.S. Squirrell, R.S.; Aeolian sand strip mobility and protodune development on a drying beach: Examining surface moisture and surface roughness patterns measured by terrestrial laser scanning. *Earth Surf. Process. Landf.* **2011**, *4*, 513–522.
5. Nagihara, S.; Mulligan, K.R.; Xiong, W. Use of a three-dimensional laser scanner to digitally capture the topography of sand dunes in high spatial resolution. *Earth Surf. Process. Landf.* **2004**, *3*, 391–398.
6. Nelson, A.; Reuter, H.I.; Gessler, P. DEM Production Methods and Sources. In *Geomorphometry Concepts, Software, Applications*; Hengl, T., Reuter, H.I., Eds.; Elsevier: Amsterdam, The Netherlands, 2009; pp. 65–85.
7. Houser, C.; Hapke, C.; Hamilton, S. Controls on coastal dune morphology, shoreline erosion and barrier island response to extreme storms. *Geomorphology* **2008**, *3*, 223–240.
8. Sallenger, A.H.; Krabill, W.B.; Swift, R.N.; Brock, J.; List, J.; Hansen, M.; Holman, R.A.; Manizade, S.; Sontag, J.; Meredith, A.; *etc*. Evaluation of airborne topographic lidar for quantifying beach changes. *J. Coastal Res.* **2003**, *1*, 125–133.
9. Stockdonf, H.F.; Sallenger Jr., A.H.; List, J.H.; Holman, R.A. Estimation of shoreline position and change using airborne topographic lidar data. *J. Coast. Res.* **2002**, *18*, 502–513.
10. Snavely, N,; Seitz,; S.M, Szeliski, R. Photo tourism: Exploring photo collections in 3D. *ACM Trans. Graph.* **2006**, *25*, 835–846.
11. Snavely, N. Scene Reconstruction and Visualization from Internet Photo Collections. Ph.D. Thesis, University of Washington, Seattle, WA, USA, 2008.
12. Ullman, S. The interpretation of structure from motion. *Proc. R. Soc. Lond. B* 1979, *203*, 405–426.
13. Tomasi, C.; Kanade, T. Shape and motion from image streams under orthography: A factorization method. *Int. J. Comput. Vis.* **1992**, *9*, 137–154.

14. Poelman, C.J.; Kanade, T. A paraperspective factorization method for shape and motion recovery. *IEEE. Trans. Pattern Anal. Mach. Intell.* **1997**, *19*, 97–108.

15. Frahm, J-M.; Pollefeys, M.; Lazebnik, S.; Gallup, D.; Clipp, B.; Raguram, R.; Wu, C.; Zach, C.; Johnson, T. Fast robust large-scale mapping from video and internet photo collections. *ISPRS J. Photogramm. Remote Sens.* **2010**, *65*, 538–549.

16. Lingua, A.; Marenchino, D.; Nex, F. Performance analysis of the SIFT operator for automatic feature extraction and matching in photogrammetric applications. *Sensors* **2009**, *9*, 3745–3766.

17. Barazzetti, L.; Remondino, F.; Scaioni, M.; Brumana, R. Fully Automatic UAV Image-Based Sensor Orientation. In Proceedings of the 2010 Canadian Geomatics Conference and Symposium of Commission I, Calgary, AB, Canada, 15–18 June 2010.

18. Baltsavias, E.; Gruen, A.; Zhang, L.; Waser, L.T. High-quality image matching and automated generation of 3D tree models. *Int. J. Remote Sens.* **2008**, *29*, 1243–1259.

19. Fonstad, M.A.; Dietrich, J.T.; Courville, B.C.; Jensen, J.L; Carbonneau, P.E. Topographic structure from motion: A new development in photogrammetric measurement. *Earth Surf. Process. Landf.* **2013**, *38*, 421–430.

20. Rango, A.; Laliberte, A.; Herrick, J.E.; Winters, C.; Havstad. K.; Steele, C.; Browning, D. Unmanned aerial vehicle-based remote sensing for rangeland assessment, monitoring, and management. *J. Appl. Remote Sens.* **2009**, *3*, 033542.

21. Verhoeven, G. Providing an archaeological bird's eye view—An overall picture of ground-based means to execute low-altitude aerial photography (LAAP) in archaeology. *Archaeol. Prospect.* **2009**, *16*, 233–249.

22. Verhoeven, G.; Loenders, J.; Vermeulen, F.; Docter, R. Helikite aerial photography (HAP)—A versatile means of unmanned, radio-controlled, low-altitude aerial archaeology. *Archaeol. Prospect.* **2009**, *16*, 125–138.

23. Mathews, A.; Jensen, J. Visualizing and quantifying vineyard canopy LAI using an unmanned aerial vehicle (UAV) collected high density structure from motion point cloud. *Remote Sens.* **2013**, *5*, 2164–2183.

24. D'Oleire-Oltmanns, S.; Marzolff, I.; Peter, K.; Ries, J. Unmanned aerial vehicle (UAV) for monitoring soil erosion in Morocco. *Remote Sens.* **2012**, *4*, 3390–3416.

25. Wallace, L.; Lucieer, A.; Watson, C.; Turner, D. Development of a UAV-LiDAR system with application to forest inventory. *Remote Sens.* **2012**, *4*, 1519–1543.

26. Hunt, E.; Hively, W.; Fujikawa, S.; Linden, D.; Daughtry, C.; McCarty, G. Acquisition of NIR-Green-Blue digital photographs from unmanned aircraft for crop monitoring. *Remote Sens.* **2010**, *2*, 290–305.

27. Fonstad, M.A.; Marcus, W.A. High resolution, basin extent observations and implications for understanding river form and process. *Earth Surf. Process. Landf.* **2010**, *35*, 680–698.

28. Turner, D.; Lucieer, A.; Watson, C. An automated technique for generating georectified mosaics from ultra-high resolution unmanned aerial vehicle (UAV) imagery, based on structure from motion (SfM) point clouds. *Remote Sens.* **2012**, *4*, 1392–1410.

29. Harwin, S.; Lucieer, A. Assessing the accuracy of georeferenced point clouds produced via multi-view stereopsis from unmanned aerial vehicle (UAV) imagery. *Remote Sens.* **2012**, *4*, 1573–1599.

30. Rosnell, T.; Honkavaara, E. Point cloud generation from aerial image data acquired by a quadrocopter type micro unmanned aerial vehicle and a digital still camera. *Sensors* **2012**, *12*, 453–480.

31. Bryson, M.; Johnson-Roberson, M.; Murphy, R.J.; Bongiorno, D. Kite aerial photography for low-cost, ultra-high spatial resolution multi-spectral mapping of intertidal landscapes. *PloS One* **2013**, *8*, e73550.

32. Wheaton, J.M.; Brasington, J.; Darby, S.E.; Sear, D.A. Accounting for uncertainty in DEMs from repeat topographic surveys: Improved sediment budgets. *Earth Surf. Process. Landf.* **2010**, *35*, 136–156.

33. Teatini, P.; Ferronato, M.; Gambolati, G.; Bertoni, W.; Gonella, M. A century of land subsidence in Ravenna, Italy. *Env. Geol*. **2005**, *47*, 831–846.

34. Carbognin, L.; Tosi, L. Interaction between climate changes, eustacy and land subsidence in the North Adriatic Region, Italy. *Mar. Ecol. Prog. Ser.* **2002**, *23*, 38–50.

35. Agisoft PhotoScan. *User Manual: Professional Edition*; Version 0.9.1; AgiSoft LLC: Petersburg, Russia, 2013.

36. Seitz, S.; Curless, B.; Diebel, J.; Scharstein, D.; Szeliski, R. A Comparison and Evaluation of Multi-View Stereo Reconstruction Algorithms. In Proceedings of the 2006 IEEE Computer Society Conference on Computer Vision and Pattern, Washington, DC, USA, 17–22 June 2006; pp. 519–528.

37. Szeliski, R. *Computer Vision: Algorithms and Applications*; Springer-Verlag: London, UK, 2010.

38. Verhoeven, G. Taking computer vision aloft—Archaeological three-dimensional reconstructions from aerial photographs with PhotoScan. *Archaeol. Prospect.* **2011**, *18*, 67–73.

39. Montreuil, A.; Joanna, B.; Chandler, J. Detecting seasonal variations in embryo dune morphology using a terrestrial laser scanner. *J. Coast. Res*. **2013**, *65*, 1313–1318.